A novel method to derive the aerosol hygroscopicity parameter based only on measurements from a humidified nephelometer system

Ye Kuang[1], ChunSheng Zhao[1], JiangChuan Tao[1], YuXuan Bian[2], Nan Ma[3], Gang Zhao[1]

[1]{Department of Atmospheric and Oceanic Sciences, School of Physics, Peking University, Beijing, China}

[2]{State Key Laboratory of Severe Weather, Chinese Academy of Meteorological Sciences}

[3]{Leibniz Institute for Tropospheric research, Leipzig, Germany}

*Correspondence to: C. S. Zhao (zcs@pku.edu.cn)

Abstract

Aerosol hygroscopicity is crucial for understanding roles of aerosol particles in atmospheric chemistry and aerosol climate effects. Light scattering enhancement factor $f(\mathrm{RH}, \lambda)$ is one of the parameters describing aerosol hygroscopicity which is defined as $f(\mathrm{RH}, \lambda) = \sigma_{sp}(RH, \lambda)/\sigma_{sp}(dry, \lambda)$ where $\sigma_{sp}(RH, \lambda)$ or $\sigma_{sp}(dry, \lambda)$ represents σ_{sp} at wavelength λ under certain RH or dry conditions. Traditionally, an overall hygroscopicity parameter κ can be retrieved from measured $f(\mathrm{RH}, \lambda)$, hereinafter referred to as $\kappa_{f(\mathrm{RH})}$, by combining concurrently measured particle number size distribution (PNSD) and mass concentration of black carbon. In this paper, a new method is proposed to directly derive $\kappa_{f(\mathrm{RH})}$ based only on measurements from a three-wavelength humidified nephelometer system. The advantage of this newly proposed approach is that $\kappa_{f(\mathrm{RH})}$ can be estimated without any additional information about PNSD and black carbon. This method is verified with measurements from two different field campaigns. Values of $\kappa_{f(\mathrm{RH})}$ estimated from this new method agree very well with those retrieved by using the traditional method, all points lie nearby 1:1 line, the square of correlation coefficient between them is 0.99. The verification results demonstrate that this newly proposed method of deriving $\kappa_{f(\mathrm{RH})}$ is applicable in different sites and seasons.

1. Introduction

Atmospheric aerosol particles play vital roles in visibility, energy balance and the hydrological cycle of the Earth-atmosphere system and have attracted a lot of attention in recent decades. Aerosol particles suspended in the atmosphere directly influence radiative transfer of solar radiation and indirectly affect cloud properties, therefore, have large impacts on climate change. Especially, uncertainties in direct aerosol radiative forcing due to anthropogenic aerosols and in aerosol indirect forcing caused by aerosol interaction with clouds contribute most to the total uncertainty in climate forcing (Boucher et al., 2013). One of the most important factors affect these uncertainties is the interaction between aerosol particles and ambient atmospheric water vapour (Zhao et al., 2006;Kuang et al., 2016b). Under supersaturated conditions, aerosol particles serve as cloud condensation nuclei (CCN) and hence influence cloud properties. Under subsaturated conditions, with respect to typical aerosol compositions, water usually constitutes about half of the aerosol mass at a relative humidity (RH) of 80% with substantially higher water mass fractions existing at RH values above 90% for most ambient aerosol (Bian et al., 2014).The water content of aerosol and cloud droplets depend on both the ambient RH and hygroscopicity of the aerosol chemical constituents.

Traditionally, the Köhler theory (Petters and Kreidenweis, 2007) is widely used to describe the hygroscopic growth of aerosol particles and successfully used in laboratory studies for single component and some multicomponent particles. In order to account for the mixed organic and inorganic composition of ambient aerosol, Petters and Kreidenweis (2007) proposed a modified version of Köhler theory called κ-Köhler theory to describe a single aerosol hygroscopic growth parameter, κ. The κ-Köhler equation, expressed in terms of the diameter growth factor, g(RH), is given in equation (1) below:

$$\frac{RH}{100} = \frac{g^3-1}{g^3-(1-\kappa)} \cdot \exp\left(\frac{4\sigma_{s/a} \cdot M_{water}}{R \cdot T \cdot D_d \cdot g \cdot \rho_w}\right) \qquad (1)$$

where g corresponds to g(RH), D_d is the dry diameter, $\sigma_{s/a}$ is the surface tension of solution/air interface, T is the temperature, M_{water} is the molecular weight of water, R is the universal gas constant, ρ_w is the density of water, and κ is the hygroscopicity parameter. This theory is not only applicable to single-component aerosol particles, but also to multicomponent aerosol particles. With regard to a multicomponent aerosol particle, the Zdanovskii, Stokes, and Robinson assumption can be applied. The hygroscopicity parameter κ of multicomponent aerosol particle can be derived by using the following formula: $\kappa = \sum_i \varepsilon_i \cdot \kappa_i$, where κ_i and ε_i represent the hygroscopic parameter

and volume fraction of each component. This hygroscopicity parameter κ has received much attentions and turns out to be a very effective parameter to study aerosol hygroscopicity. This hygroscopicity parameter κ makes the comparison of the aerosol hygroscopicity at different sites around the world and different time periods more convenient. In addition, hygroscopicity parameter κ also facilitates the intercomparison of aerosol hygroscopicity derived from different techniques and measurements made at different RHs. This hygroscopicity parameter κ is widely used to account the influence of aerosol hygroscopic growth on aerosol optical properties as well as aerosol liquid water contents (Tao et al., 2014;Kuang et al., 2015;Brock et al., 2016;Bian et al., 2014;Zieger et al., 2013) and to examine the role of aerosol hygroscopicty in CCN (Chen et al., 2014;Gunthe et al., 2009;Ervens et al., 2010). The derived κ values from field campaigns and laboratory studies will further our understanding in aerosol hygroscopicity and help estimate the influences of aerosol hygroscopic growth on different aspects of atmospheric processes.

The Humidity Tandem Differential mobility Analyzer (HTDMA) measures the aerosol diameter hygroscopic growth as a function of RH. The aerosol hygroscopicity parameter κ can be directly derived from measurements of HTDMA by applying equation (1) (Liu et al., 2011;Wu et al., 2016). HTDMA systems can provide insights into the aerosol hygroscopicity at different aerosol diameters, however, they can only be used to derive aerosol hygroscopicity parameter κ within certain size range (usually less than 300 nm). HTDMA systems are not capable of providing more details about aerosol hygroscopicity of aerosol particles which contribute most to aerosol optical properties and aerosol liquid water contents (their diameters usually ranging from 200 nm to 1μm) (Ma et al., 2012;Bian et al., 2014). The effect of aerosol water uptake on the aerosol particle light scattering (σ_{sp}) is usually measured with a humidified nephelometer system. Measurements from a humidified nephelometer system can also be used to calculate the aerosol hygroscopicty parameter κ if the dry aerosol particle number size distribution (PNSD) is measured simultaneously (Chen et al., 2014). The scattering enhancement factor $f(\text{RH},\lambda)$, defined as $f(\text{RH},\lambda) = \sigma_{sp}(RH,\lambda)/\sigma_{sp}(dry,\lambda)$, characterizes changes in the aerosol scattering coefficient with RH, $\sigma_{sp}(RH,\lambda)$ or $\sigma_{sp}(dry,\lambda)$ represents σ_{sp} at wavelength λ at a certain RH or under dry conditions. In this research, $f(\text{RH})$ is referred to as $f(\text{RH}, 550\,\text{nm})$. The nephelometer measures aerosol optical properties of the entire aerosol size distribution. Thus, κ calculated from f(RH) measurements can be understood as an optically weighted κ and represents the overall hygroscopicty of ambient aerosol particles. This κ is more

suitable for being used to account the influences of aerosol hygroscopic growth on aerosol optical properties compared to aerosol hygroscopicity derived from HTDMA and CCN measurements. Traditionally, derivation of κ from f(RH) measurements requires aerosol PNSD as well as black carbon (BC) measurements to determine the imaginary part of the refractive index. As PNSD and BC measurements are expensive, their availability in field campaigns are limited.

In this paper we use measurements from a field campaign on the North China Plain (NCP) to derive κ values using 3 methods. The first 2 methods derive κ from aerosol diameter hygroscopic growth and the third method derives an aerosol optical parameterization of κ. Method 1, labeled as $\kappa_{f(RH)}$, derives κ from aerosol PNSD, BC and nephelometer f(RH) measurements. Method 2, defined as κ_{250}, derives κ from g(RH) measurements of aerosol particles with diameter of 250 nm, using a High-Humidity Differential Mobility Analyzer (HH-TDMA). HH-TDMA is a system very similar to HTDMA but is capable of operating at higher RH points (Liu et al., 2011). Method 3, defined as κ_{sca}, is an empirical determination of κ using only nepehelometer measurements of the aerosol scattering coefficient as a function of RH.

Based on detailed analysis about the relationship between $\kappa_{f(RH)}$ and κ_{sca}, a novel method to directly derive $\kappa_{f(RH)}$ based only on measurements from a humidified nephelometer system is proposed. This newly proposed approach makes it more convenient and cheaper for researchers to conduct aerosol hygroscopicity research with $f(RH)$ measurements.

2. Site description and instruments

Datasets from five field campaigns are used in this paper. The five campaigns are conducted at four different measurement sites of the North China Plain (NCP) (Wangdu, Xianghe and Gucheng in Hebei province and Wuqing in Tianjin, and site locations are shown in Fig.S1). Time periods and used datasets from these filed campaigns are listed in Table 1.

During these field campaigns, sampled aerosol particles have aerodynamic diameters less than 10 μm (selected by passing through an impactor). Aerosol PNSDs with particle diameter ranging from 3nm to 10μm were jointly measured by a Twin Differential Mobility Particle Sizer (TDMPS, Leibniz-Institute for Tropospheric Research (IfT), Germany; Birmili et al. (1999)) or a scanning mobility particle size spectrometer (SMPS) and an Aerodynamic Particle Sizer (APS, TSI Inc., Model 3321) with a temporal resolution of 10 minutes. The mass concentrations of BC were measured using a Multi-

angle Absorption Photometer (MAAP Model 5012, Thermo, Inc., Waltham, MA USA) or an aethalometer called AE33 (Drinovec et al., 2015). The aerosol light scattering coefficients (σ_{sp}) at three wavelengths were measured using a TSI 3563 nephelometer (Anderson and Ogren, 1998) or an Aurora 3000 nephelometer (Müller et al., 2011).

A humidified nephelometer system consists of two nephelometers and a humidifier was used in Wangdu and Gucheng campaigns. For the humidified nephelometer systems that we have designed, they only scan the hydration branch of the aerosol hygroscopic growth. The humidifier humidified the sample air through a Gore-Tex tube. The water vapor penetrates through the Gore-Tex tube, which is surrounded by a circulating water layer in a stainless steel tube. The temperature cycle of the circulating water layer was specified and controlled by a water bath. During Wangdu campaign, only one water bath was used, for each RH scanning cycle, the temperature cycle was fixed. Thus, the RH range of each cycle will change. Since the room temperature of the container was relatively stable during Wangdu campaign, the RH points of $f(\text{RH})$ cycles range from about 50% to about 90%, and each cycle lasted about 45 minutes. However, one cycle cost about 90 minutes because after each cycle was finished, the water bath needed about another 45 minutes to cool. During Gucheng campaign, this problem is solved by using two water baths and they provided circulating water alternatively for the humidifier. The corresponding temporal resolution of $f(\text{RH})$ cycles was about 45 minutes. In addition, a control software system was developed and can make sure the RH scans within certain RH range. During Gucheng campaign, the RH points of each $f(\text{RH})$ cycle range from 45% to 90%. During Wangdu campaign, the two nephelometers operated in series, used nephelometer was TSI 3563. During Gucheng campaign, the two nephelometers operated in parallel, used nephelometer was Aurora 3000. In the following, we refer the nephelometer which measures σ_{sp} in dry state and the nephelometer which measures σ_{sp} at different RH points as dry Neph and wet Neph, respectively. Two combined RH and temperature sensors (Vaisala HMP110; accuracy of $\pm 0.2\,°C$ and $\pm 1.7\,\%$ for RH ranges from 0 to 90 %, respectively, and accuracy of $\pm 2.5\,\%$ for RH ranges from 90 % to 100 % according to the manufacturer) are placed at the inlet and outlet of the wet Neph, and the measured RHs and temperatures are defined as RH_1/T_1 and RH_2/T_2, respectively. The dew points at the inlet and outlet of wet Neph were calculated using the measured RH_1/T_1 and RH_2/T_2, and the average value was considered as the dew point of the sample air. The sample RH can be calculated through the derived dew point and the sample temperature which is measured by the sensor inside the

sample cavity of the nephelometer. During Wangdu campaign, measurements from the humidified nephelometer system were only available from 21 June, 2014, to 1 July , 2014. During the two campaigns, the two nephelometers were calibrated every two weeks. The manufacturer of HMP110 suggests that the sensors should be calibrated yearly. We didn't calibrate the used HMP110 sensors during the two campaigns because they only have been used less than three months, and results of cross checks showed that they agree well with each other. The sample RHs in the dry Neph were about 20% and about 8% during Wangdu and Gucheng campaigns, respectively.

Dataset includes aerosol PNSDs at dry state, mass concentrations of BC and σ_{sp} values of different wavelengths from the following four campaigns which are listed in Table 1 are referred to as dataset D1: two campaigns conducted in Wuqing, Xianghe campaign, Wangdu campaign before 21 June, 2014. Note that σ_{sp} values of dataset D1 are not corrected. However, for σ_{sp} values shown in Fig.1, the truncation errors are corrected using Mie theory with measured PNSD and mass concentrations of BC.

During Wangdu campaign, the growth factors of aerosol particles at six selected particle diameters (30 nm, 50 nm, 100 nm, 150nm, 200 nm and 250 nm) at 98% RH condition were obtained from the measurements of the HH-TDMA (Leibniz-Institute for Tropospheric Research (IfT), Germany; Hennig et al. (2005)). Detailed information about HH-TDMA measurements please refer to Liu et al. (2011)

3. Methodology

3.1 Calculations of hygroscopicity parameter κ from $f(\text{RH})$ measurements and HH-TDMA

Research of Chen et al. (2014) demonstrated that if the PNSD at dry state is measured, then measurements of $f(\text{RH})$ can be used to derive the aerosol hygroscopicity parameter κ by conducting an iterative calculation with the Mie theory and the κ-K$\ddot{o}$hler theory. To reduce the influence of random errors of observed $f(\text{RH})$ at a certain RH, all valid $f(\text{RH})$ measurements in a complete humidifying cycle is used in the derivation algorithm. The retrieved κ is the κ value which can be used to best fit the observed $f(\text{RH})$ curve, labelled as $\kappa_{f(RH)}$, and this method of deriving κ is Method 1. Details about this retrieval algorithm is described in Chen et al. (2014). Of particular note is that in this research the mass concentration of BC is also considered in the retrieval algorithm to account for the influence of BC on refractive indices of aerosol particles at different sizes. During the simulating process, aerosol components are divided into two classes in terms of their optical properties:

the light absorbing component (i.e. BC) and less absorbing components (comprising inorganic salts and acids such as sulfates, nitrates, ammoniums, as well as most of the organic compounds). The BC is considered to be homogeneously mixed with other aerosol components, and the mass size distribution of BC used in Ma et al. (2012) which is observed on the NCP is used in this research to account the mass distributions of BC at different particle sizes. The used refractive index and density of BC are $1.80 - 0.54i$ and $1.5 \text{g } cm^{-3}$ (Kuang et al., 2015). Used refractive indices of non light-absorbing aerosol components (other than BC) and liquid water are $1.53 - 10^{-7}i$ (Wex et al., 2002) and $1.33 - 10^{-7}i$ (Seinfeld and Pandis, 2006), respectively. The flow chart about this retrieval algorithm is also introduced in the supporting information, please refer to Fig.S2 for more details.

The HH-TDMA measures hygroscopic growth factors of particles at different sizes at 98% RH condition. The measured hygroscopic factors can be directly related to κ with equation (1). For a specified size of selected aerosol particles, a distribution of growth factors can be measured, and thus can be used to derive a probability distribution of κ and finally come to the calculation of average κ value corresponding to this size of aerosol particles. The method on how to derive average κ value of certain size of aerosol particles from HH-TDMA measurements is elaborately described in Liu et al. (2011). In this research κ values derived from g(RH) measurements of aerosol particles with diameter of 250 nm are used, defined as κ_{250}. This method of deriving κ is Method 2.

3.2 Parameterization schemes for $f(\text{RH})$

The most frequently used $f(\text{RH})$ parameterization scheme is a power-law function which is known as "gamma" parameterization (Hänel, 1981) and the formula of this single-parameter representation is written as the following:

$$f(\text{RH}) = \left[\frac{(100 - RH_0)}{100 - RH} \right]^{\gamma} \quad (2)$$

where RH_0 is the RH of dry condition, and γ is a parameter fitted to the observed $f(\text{RH})$. In this study, we estimated γ values with observed $f(\text{RH})$ curves and for the first time to our knowledge, we further examined the relationship between γ and $\kappa_{f(RH)}$.

Recently, a new physically based single-parameter representation was proposed by Brock et al. (2016) to describe $f(\text{RH})$. Their results demonstrated that this proposed parameterization scheme can better describe $f(\text{RH})$ than the widely used gamma power-law approximation (Brock et al., 2016). The formula of this new scheme is written as:

206
$$f(\text{RH}) = 1 + \kappa_{sca}\frac{RH}{100-RH} \qquad (3)$$

207   where κ_{sca} is a parameter fits $f(\text{RH})$ best. Regardless of the curvature effects for particle diameters

208   larger than 100 nm, the hygroscopic growth factor for aerosol particles can be approximately expressed

209   as the following (Brock et al., 2016): $gf_{diam} \cong (1+\kappa\frac{RH}{100-RH})^{1/3}$. Moreover, σ_{sp} is usually

210   approximately proportional to total aerosol volume (Pinnick et al., 1980) which means that the relative

211   change in σ_{sp} due to aerosol water uptake is roughly proportional to relative change in aerosol volume.

212   The enhancement factor in volume can be expressed as the cube of gf_{diam}, thus lead to the formula

213   form of $f(\text{RH})$ expressed in equation (3)..

214   During processes of measuring $f(\text{RH})$, the sample RH in the dry Neph (RH_0) is not zero.

215   According to equation (3), the measured $f(\text{RH})_{measure} = \frac{f(\text{RH})}{f(RH_0)}$ should be fitted using the following

216   formula:

217
$$f(\text{RH})_{measure} = (1 + \kappa_{sca}\frac{RH}{100-RH})\big/(1 + \kappa_{sca}\frac{RH_0}{100-RH_0}) \qquad (4)$$

218   The method of calculating κ_{sca} by curve fitting using equation (4) is called Method 3. These

219   two parameterization schemes which are introduced here are referred to as γ-Method and κ_{sca}-

220   Method respectively in the following paragraphs.

221   **4.   Results and discussions**

222   **4.1 Derived κ values from $f(\text{RH})$ and HH-TDMA measurements**

223   During this field campaign, the aerosol physical, chemical and optical properties are

224   synergistically observed with different types of instruments. They provide valuable datasets to perform

225   an insightful analysis about aerosol hygroscopicity and its relationship with other aerosol properties.

226   The time series of σ_{sp} at 550 nm at dry state are shown in Fig.1a.. The results show that this

227   observation period has experienced varying degrees of pollution levels, with σ_{sp} at 550 nm ranging

228   from 15 to 1150 Mm^{-1}.Values of $\kappa_{f(\text{RH})}$ derived from Method 1 are shown in Fig.1b. During

229   deliquescence f(RH) exhibits an abrupt increase between RH values of 60-65%. As such, only f(RH)

230   data points with RH >70% were used in determination of $\kappa_{f(\text{RH})}$ when deliquescence was apparent.

231   For f(RH) cycles without deliquescence, all f(RH) points are used in the retrieval algorithm with RH

232   ranges of about 50% to 90%. The results demonstrate that $\kappa_{f(\text{RH})}$ lies between 0.06 and 0.51, with an

233   average of 0.32. The lowest $\kappa_{f(\text{RH})}$ values are found when the air quality is relatively clean (σ_{sp} at

550 nm is lower than 100 Mm^{-1}) on 27 and 28 June. During these two days, organic matter dominates the mass concentration of PM2.5 which results in the low hygroscopicity of aerosol particles (Kuang et al., 2016a). On the contrary, the largest $\kappa_{f(RH)}$ values are found during periods when deliquescent phenomena occur and inorganic chemical compositions dominate the mass concentrations of PM2.5, especially, sulfate is highly abundant during these periods. Of particular note is that during relatively polluted periods (σ_{sp} at 550 nm larger than 100 Mm^{-1}) aerosol particles are generally very hygroscopic which imply that aerosol water uptake can exert significant impacts on regional direct aerosol radiative effect and ambient visibility during this observation period.

On the basis of the average size-resolved κ distribution from Haze in China (HaChi) campaign (Liu et al., 2014), κ values change a lot for aerosol particles whose diameters are less than 250 nm, however, κ values vary relatively smaller for aerosol particles whose diameter range from 250 nm to 1 μm. In addition, the results from HaChi campaign also demonstrate that aerosol particles whose diameter range from 200 nm to 1 μm usually contribute more than 80% to σ_{sp} at 550 nm during summer on the NCP (Ma et al., 2012). That is, $\kappa_{f(RH)}$ may share similar magnitude with κ_{250}. To compare κ values derived from Method 1 and Method 2values of κ_{250} are also shown in Fig.1b. During this observation period, values of κ_{250} range from 0.11 to 0.56, with an average of 0.34 which is very close to average κ_{250} observed during HaChi campaign (Liu et al., 2011). The results shown in Fig.1b suggest that, in general, $\kappa_{f(RH)}$ values agree well with κ_{250} values, however, are usually lower than κ_{250} values. To quantitatively compare these two types of κ values, they are plotted against each other and shown in Fig.2. It can be seen that they are highly correlated but overall, the κ_{250} values are higher than $\kappa_{f(RH)}$ values, and the average difference between κ_{250} and $\kappa_{f(RH)}$ is 0.02. The statistical relationship between κ_{250} and $\kappa_{f(RH)}$ is also shown in Fig.2.This relationship may be useful for researchers if they want to estimate the influences of aerosol water uptake on aerosol optical properties and aerosol liquid water contents when only HH-TDMA or HTDMA measurements are available.

A model experiment is conducted to better understand the relationship between κ_{250} and $\kappa_{f(RH)}$. During HaChi campaign, size-resolved κ distributions are derived from measured size-segregated chemical compositions (Liu et al., 2014) and their average is used in this experiment to account the size dependence of aerosol hygroscopicity which is shown in Fig. 3a. With this fixed average size-resolved κ distribution, all observed PNSDs at dry state along with mass concentrations of BC from

264   dataset D1 are used to simulate the retrieval of $\kappa_{f(\text{RH})}$ under different PNSD and BC conditions. The

265   used PNSDs shown in Fig.3b indicate that large varying types of PNSDs are considered in the

266   simulative experiment. As to the simulating process, with given PNSD, mass concentration of BC and

267   size-resolved κ distribution. The first step is simulating $f(\text{RH})$ points using Mie theory and κ-

268   Köhler theory with RH range of 50% to 90% and the RH interval is 10%. The second step is retrieving

269   corresponding $\kappa_{f(\text{RH})}$ using the procedure of Method 1. The κ value at particle diameter of 250 nm

270   of the used size-resolved κ distribution is the corresponding κ_{250}. The probability distribution of

271   simulated $\kappa_{f(\text{RH})}$ is also shown in Fig.3a. The standard deviation of retrieved $\kappa_{f(\text{RH})}$ is about 0.01

272   which suggests that if the size-resolved κ distribution is fixed, then $\kappa_{f(\text{RH})}$ varies little. Due to

273   $\kappa_{f(\text{RH})}$ represents an overall, size-integrated κ, it is clearly shown in Fig.3a that in most cases $\kappa_{f(\text{RH})}$

274   values are located between κ values of aerosol particles ranging from 200 nm to 1μm. Moreover,

275   about 70% of simulated $\kappa_{f(\text{RH})}$ values are less than κ_{250} which to some extent explains the observed

276   difference between κ_{250} and $\kappa_{f(\text{RH})}$ mentioned before. However, the simulated average difference

277   between κ_{250} and average $\kappa_{f(\text{RH})}$ is about 0.01 which is   less than the observed averaged difference

278   between κ_{250} and $\kappa_{f(\text{RH})}$ which is 0.02. Especially, when $\kappa_{f(\text{RH})}$ values are relatively lower ($<$

279   0.25), the κ_{250} is systematically higher than $\kappa_{f(\text{RH})}$. Except that uncertainties from measurements of

280   instruments, for example, the uncertainty of RH in measurements of HH-TDMA and uncertainties of

281   measuring $f(\text{RH})$ (details about the uncertainty sources of $f(\text{RH})$ measurements can be found in

282   the paper published by Titos et al. (2016)), there are other two reasons may be associated with the

283   discrepancy between κ_{250} and $\kappa_{f(\text{RH})}$. The first one is that configurations of size-resolved κ

284   distributions and PNSDs during this field campaign are far different from the model experiment. The

285   second one is that in the real atmosphere, κ values at different RH conditions may be different (You

286   et al., 2014) and most of $f(\text{RH})$ measurements are conducted when RH is lower than 90%, however,

287   the measurements of HH-TDMA are conducted when RH is equal to 98% . Overall, the observed

288   general consistency between κ values derived from measurements of $f(\text{RH})$ and HH-TDMA

289   confirms the reliability of κ values derived from $f(\text{RH})$ measurements.

290   **4.2 Relationships between κ derived from $f(\text{RH})$ measurements and $f(\text{RH})$ fitting**

291   **parameters**

292   In the previous section, derived $\kappa_{f(\text{RH})}$ values are characterized and compared with κ_{250} values.

293   These results demonstrated that derived $\kappa_{f(RH)}$ values can commendably represent variations of

294   aerosol hygroscopicty of ambient aerosol populations. In this section, the relationship between derived

295    $\kappa_{f(RH)}$ values and $f(RH)$ fitting parameters are further examined to investigate their relationships.

296   Two parameterization schemes of $f(RH)$ are discussed in this paper, including the γ-Method

297   and the newly proposed κ_{sca}-Method. Values of γ and κ_{sca} are fitted from observed $f(RH)$ cycles.

298   For cycles during deliquescent periods, only $f(RH)$ points with RH higher than 70% are used to

299   perform fitting processes. The relationship between $\kappa_{f(RH)}$ and γ is investigated and shown in

300   Fig.4a. It is found that an approximately linear relationship exists (square of correlation coefficient is

301   0.90) between $\kappa_{f(RH)}$ and γ, especially when $\kappa_{f(RH)}$ is larger than 0.2. During this field campaign,

302   fitted γ ranges from 0.13 to 0.56 with an average of 0.41.

303   During this field campaign, fitted κ_{sca} ranges from 0.05 to 0.36 with an average of 0.22. The

304   relationship between $\kappa_{f(RH)}$ and κ_{sca} is also investigated and shown in Fig.4b. It is found that a

305   strong linear relationship also exists (square of correlation coefficient is 0.97) between $\kappa_{f(RH)}$ and

306   κ_{sca}. The statistically fitted line almost passes though zero point which implies that a proportional

307   relationship may exist between $\kappa_{f(RH)}$ and κ_{sca}. This strong correlation should be intrinsic due to

308   the idea of κ_{sca}-Method is from the linkage between total aerosol volume and σ_{sp} as introduced in

309   Sect.3.2 and the increase of total aerosol volume due to aerosol water uptake is directly linked to the

310   overall aerosol hygroscopicity parameter κ. It seems that this promising linear relationship can help

311   bridge the gap between $f(RH)$ and κ. However, results from Brock et al. (2016) imply that the

312   relationship between $\kappa_{f(RH)}$ and κ_{sca} is much more sophisticated and it is affected by both aerosol

313   hygroscopicity and PNSD at dry state. In the paper published by Brock et al. (2016), κ_{ext} (a parameter

314   determined from measurements of the aerosol extinction coefficient as a function of RH using formula

315   form of equation (2)) and κ_{chem} (a constant κ determined from chemical constituents of entire

316   aerosol population) are used and correspond to κ_{sca} and $\kappa_{f(RH)}$ in this research, the difference

317   between κ_{ext} and κ_{sca} is that κ_{ext} is used to fit the light enhancement factor of aerosol extinction

318   coefficient, κ_{chem} and $\kappa_{f(RH)}$ actually means the same because both them are overall and size

319   independent hygroscopicity parameters. Results from Brock et al. (2016) concluded that the ratio

320    $\kappa_{ext}/\kappa_{chem}$ generally lies between 0.6 to 1 which implies that the ratio $\kappa_{sca}/\kappa_{f(RH)}$ (in the following,

321   this ratio is referred to as R_{κ}) also should have large variations and may share a similar range of

322   variability. By revisiting the relationship between $\kappa_{f(RH)}$ and κ_{sca} found in this research, it can be

323   found that R_κ during this field campaign ranges from 0.58 to 0.77 with an average of 0.69. This result

324   suggests that if we directly establish a linkage between $\kappa_{f(RH)}$ and κ_{sca} with an average R_κ can

325   result in a non-negligible bias (relative difference can reach about 15%). Besides, this range of R_κ

326   only represents the relationship between $\kappa_{f(RH)}$ and κ_{sca} during a short time period and at only one

327   site.

328   To better understand the relationship between $\kappa_{f(RH)}$ and κ_{sca}, all PNSDs at dry state (shown

329   in Fig.3a) along with mass concentrations of BC from dataset D1 are used to simulate the relationship

330   between $\kappa_{f(RH)}$ and κ_{sca} with Mie and κ-Köhler theories. The aim of including PNSD and BC

331   information from different campaigns is to simulate variations of R_k under different conditions.

332   During simulating processes, for each PNSD, we change $\kappa_{f(RH)}$ from 0.01 to 0.7 with an interval of

333   0.01 to examine the influence of aerosol hygroscopicity on R_κ. For each PNSD and $\kappa_{f(RH)}$, the

334   simulating processes include two steps. The first step is simulating $f(RH)$ points using Mie theory

335   and κ-Köhler theory with RH range of 50% to 90% and the RH interval is 10%. The way of treating

336   BC is same with the retrieval procedure of $\kappa_{f(RH)}$ introduced in Sect.3.1. The second step is retrieving

337   the corresponding $\kappa_{f(RH)}$ using the procedure of Method 1 and calculating κ_{sca} with Method 3.

338   Simulated results of $\kappa_{f(RH)}$ and κ_{sca} are shown in Fig.5a and the probability distribution of

339   corresponding R_κ values is shown in Fig.5b. The results show that R_κ primarily ranges from 0.5 to

340   0.84 with an average of 0.69 which is same with the average R_κ measured during Wangdu campaign.

341   These results also indicate that the relationship between $\kappa_{f(RH)}$ and κ_{sca} is much more complex than

342   a simple linear relationship and more information about aerosol properties are necessary to gain

343   insights into the variation of R_κ.

344   **4.3 A novel method to directly derive κ from measurements of a humidified nephelometer**

345   **system**

346   A robust linear relationship is   found between $\kappa_{f(RH)}$ and κ_{sca} in Sect.4.2 , however, results

347   of further analysis suggest that R_κ varies a lot. The complexity comes from that both PNSD at dry

348   state and aerosol hygroscopicity have impacts on R_κ. Generally, used nephelometer of a humidified

349   nephelometer system have three wavelengths (Titos et al., 2016) and the spectral dependence of σ_{sp}

350   is usually described by the following Ångström formula: $\sigma_{sp}(\lambda) = \beta\lambda^{-\alpha_{sp}}$, where β is the particle

351 number concentration dependent coefficient, λ is the wavelength of light and α_{sp} represents the

352 Ångström exponent of σ_{sp}. Ångström exponent can be directly inferred from the measurements

353 of σ_{sp} at different wavelengths. Of particular note is that Ångström exponent not only can be used

354 to account the spectral course of σ_{sp}, it also reveals information about PNSD. In general, larger value

355 of Ångström exponent corresponds to smaller aerosol particles. That is, Ångström exponent can

356 be a proxy of PNSD at dry state and be used in the processes of estimating the impacts of PNSD on

357 R_κ. On the other hand, with regard to aerosol hygroscopicity, although R_κ varies within certain range,

358 value of κ_{sca} can still be used to represent the overall hygroscopicity of aerosol particles.

359 Simulated R_κ values introduced in the last paragraph of Sect.4.2 are spread into a two

360 dimensional gridded plot. The first dimension is Ångström exponent with an interval of 0.02 and the

361 second dimension is κ_{sca} with an interval of 0.01, average R_κ value within each grid is represented

362 by color and shown in Fig.6a. Values of Ångström exponent corresponding different PNSDs are

363 calculated from concurrently measured σ_{sp} values at 450 nm and 550 nm from TSI 3563

364 nephelometer. Based on results shown on Fig.6a, the different impacts of aerosol hygroscopicity and

365 dry scattering Ångström exponent on R_κ can be distinguished to some extent. The results

366 demonstrate that PNSD at dry state play a more important role in the variations of R_κ than overall

367 aerosol hygroscopicty.. Overall, larger value of Ångström exponent corresponds to higher R_κ.

368 Aerosol hygroscopicty exhibits different influences on R_κ when Ångström exponent values are

369 different. On average, higher κ_{sca} corresponds to lower R_κ if Ångström exponent is smaller than

370 about 0.8 and higher κ_{sca} corresponds to higher R_κ if Ångström exponent is larger than about

371 1.6.The percentile value of standard deviation of R_κ values within each grid of Fig.6a divided by their

372 average is shown in Fig.6b. The Ångström exponent only represents an overall size property of

373 aerosol particles, the same Ångström exponent corresponds to different aerosol PNSDs. Within each

374 grid of Fig.6a, the same κ_{sca} corresponds to different combinations of aerosol PNSD and $\kappa_{f(\mathrm{RH})}$, and

375 R_κ values also change. Note that the size-dependent chemical composition also exerts influence on

376 R_k. However, if PNSD is fixed, each size-resolved κ distribution corresponds to a certain $\kappa_{f(RH)}$,

377 and $\kappa_{f(RH)}$ varies with certain range no matter how size-resolved κ distribution changes. Therefore,

378 influences of size-dependent chemical compositions on R_k are already included in the simulated

379   results of producing the look up table by varying the $\kappa_{f(RH)}$ from 0 to 0.7 for a fixed aerosol PNSD.

380   As shown in Fig.6b, in most cases, these percentile values are less than 6% (about 80%) which

381   demonstrates that R_κ varies little within each grid shown in Fig.6a. This implies that results of Fig.6a

382   can be used as a look up table to estimate R_κ. As what's introduced before, currently used

383   nephelometer of a humidified nephelometer system usually have three wavelengths (Titos et al., 2016),

384   thus can provide information about Ångström exponent, and κ_{sca} can be directly fitted from

385   observed $f(RH)$ curve. Even only one $f(RH)$ point is measured, κ_{sca} can still be calculated from

386   equation (4). Using results shown in Fig.6a as a look up table, R_κ values can be directly predicted

387   from measurements of a humidified nephelometer system. With this method, R_κ values during this

388   Wangdu field campaign are predicted (values of Ångström exponent are calculated from measured

389   σ_{sp} values at 450 nm and 550 nm under dry conditions) and compared with measured R_κ values, the

390   results are shown in Fig.7a. The Ångström exponent during this field campaign ranges from 0.63 to

391   1.96 with an average of 1.4. It can be seen from Fig.7a that majority of points lie nearby 1:1 line and

392   82% points have relative differences less than 6% which is consistent with results shown in Fig.6b.

393   This result is quite promising and can be further used to derive $\kappa_{f(RH)}$ values by combining fitted

394   κ_{sca} and predicted R_κ. This method of deriving $\kappa_{f(RH)}$ is called Method 4 and include two steps.

395   The first step is calculating Ångström exponent based on measured σ_{sp} values at 450 nm and 550

396   nm by the dry nephelometer and calculating κ_{sca} based on measured $f(RH)$ curve by the humidified

397   nephelometer system. The second step is predicting R_κ using the look up table shown in Fig.6a, and

398   then calculate $\kappa_{f(RH)}$ based on predicted R_κ and fitted κ_{sca}. The results of predicted $\kappa_{f(RH)}$ values

399   are shown in Fig.7b and a robust correlation between $\kappa_{f(RH)}$ values predicted from Method 4 and

400    $\kappa_{f(RH)}$ values derived from Method 1is achieved (the square of correlation coefficient between them

401   is 0.99). All points shown in Fig.7b lie nearby 1:1 line, average difference between $\kappa_{f(RH)}$ derived

402   fromMethod 4 and Method 1 is -0.009.

403   Datasets from Gucheng campaign are further used to verify Method 4. In this campaign, Aurora

404   3000 nephelometer is used for the humidified nephelometer system, it has three wavelengths: 450 nm,

405   525 nm and 635 nm. Values of $f(RH, \lambda)$ points correspond to wavelength of 525 nm are used to derive

406    $\kappa_{f(RH)}$ using Method 1 and Method 4, used RH range is 45% to 90%. The look up table shown in

407   Fig.6a is simulated corresponding to scattering wavelength of 550 nm, and is not suitable for being

408 used in Method 4 if the nephelometer is Aurora 3000. A new look up table is simulated corresponding

409 to scattering wavelength of 525 nm, used datasets of PNSD and BC are same with those for producing

410 the look up table shown in Fig.6a. During Gucheng campaign, the variations of $\kappa_{f(\mathrm{RH})}$ and

411 corresponding R_k with σ_{sp} at 525 nm are shown in Fig.8a. Values of $\kappa_{f(\mathrm{RH})}$ range from 0.01 to

412 0.27, with an average of 0.14. During this campaign, $\kappa_{f(\mathrm{RH})}$ is relatively lower when σ_{sp} is high.

413 Values of R_k range from 0.60 to 0.84, with an average of 0.7. Results of the comparison between

414 $\kappa_{f(\mathrm{RH})}$ derived from Method 1 and Method 4 are shown in Fig.8b. The results demonstrate that good

415 consistency is achieved between $\kappa_{f(\mathrm{RH})}$ derived from Method 1 and Method 4, the square of

416 correlation coefficient between them is 0.99.

417 The verification results of Method 4 using measurements from Wangdu and Gucheng campaigns

418 demonstrate that a quite good estimation of $\kappa_{f(\mathrm{RH})}$ can be achieved by using only measurements from

419 a humidified nephelometer system, and Method 4 is applicable at different sites and in different seasons.

420 It should be noted that the look up table shown in Fig.6a already covers large variation ranges of

421 Ångström exponent and κ_{sca}. Which means that this look up table can be used under different

422 conditions. However, it should be pointed out that the look up table shown in Fig.6a is from simulations

423 of measured continental aerosols without influences of desert dust, and it might not be suitable for

424 being used to estimate $\kappa_{f(\mathrm{RH})}$ when sea salt or dust particles prevail. In summary, this approach allows

425 researchers to directly derive aerosol hygroscopicity from measurements of $f(\mathrm{RH})$ without any

426 additional information about PNSD and BC which is quite convenient for researchers to conduct

427 aerosol hygroscopicity researches with measurements from a humidified nephelometer system.

428 **5. Conclusions**

429 In this paper, values of aerosol hygroscopicity parameter κ during Wangdu campaign are first

430 derived from measurements of $f(\mathrm{RH})$ by combining measurements of PNSD at dry state and BC.

431 The results show that during this field campaign, aerosol hygroscopicity varies a lot, and $\kappa_{f(\mathrm{RH})}$

432 ranges from 0.06 to 0.51 with an average of 0.34. Retrieved $\kappa_{f(\mathrm{RH})}$ values are further compared with

433 κ_{250} which is derived from measurements of HH-TDMA and good consistency is achieved.

434 Relationships between $\kappa_{f(\mathrm{RH})}$ and $f(\mathrm{RH})$ fitting parameters γ and κ_{sca} are further

435 investigated in Sect.4.2 which is for the first time to our knowledge. Good linear relationship is found

436 between $\kappa_{f(\mathrm{RH})}$ and κ_{sca} during Wangdu campaign. Results of detailed analysis about the

437   relationship between $\kappa_{f(\mathrm{RH})}$ and κ_{sca} demonstrate that the relationship between $\kappa_{f(\mathrm{RH})}$ and κ_{sca} is

438   complicated, and the ratio $\kappa_{sca}/\kappa_{f(\mathrm{RH})}$ (R_κ) varies a lot (0.5 to 0.84, with an average of 0.69).

439   In Sect.4.3, a look up table based on Ångström exponent and κ_{sca} is developed to estimate R_κ.

440   With this look up table, R_κ as well as $\kappa_{f(\mathrm{RH})}$ can be directly estimated from measurements of a

441   humidified nephelometer system. This method is further verified with measurements from two

442   different campaigns. The verification results demonstrate that a quite good estimation of $\kappa_{f(\mathrm{RH})}$ can

443   be achieved by using only measurements from a humidified nephelometer system, and this method is

444   applicable at different sites and in different seasons. This newly proposed novel approach allow

445   researchers to estimate $\kappa_{f(\mathrm{RH})}$ without any additional information about PNSD and BC. This new

446   finding directly links κ and $f(\mathrm{RH})$ and will make the humidified nephelometer system more

447   convenient when it comes to aerosol hygroscopicity research. Finally, findings in this research may

448   facilitate the intercomparison of aerosol hygroscopicity derived from different techniques, help for

449   parameterizing $f(\mathrm{RH})$ and predicting CCN properties with optical measurements.

450

451

Acknowledgments

453   This work is supported by the National Natural Science Foundation of China (41590872, 41375134).

454 The data used are listed in the references and a repository at http://pan.baidu.com/s/1c2Nzc5a.

455

456

457

458

References

460 Anderson, T. L., and Ogren, J. A.: Determining aerosol radiative properties using the TSI 3563 integrating nephelometer,

461 Aerosol Science and Technology, 29, 57-69, 10.1080/02786829808965551, 1998.

462 Bian, Y. X., Zhao, C. S., Ma, N., Chen, J., and Xu, W. Y.: A study of aerosol liquid water content based on hygroscopicity

463 measurements at high relative humidity in the North China Plain, Atmos. Chem. Phys., 14, 6417-6426, 10.5194/acp-14-

464 6417-2014, 2014.

465 Birmili, W., Stratmann, F., and Wiedensohler, A.: Design of a DMA-based size spectrometer for a large particle size range

466 and stable operation, Journal of Aerosol Science, 30, 549-553, 10.1016/s0021-8502(98)00047-0, 1999.

467 Boucher, O., Randall, D., Artaxo, P., Bretherton, C., Feingold, G., Forster, P., Kerminen, V.-M., Kondo, Y., Liao, H., Lohmann,

468 U., Rasch, P., Satheesh, S. K., Sherwood, S., Stevens, B., and Zhang, X. Y.: Clouds and Aerosols, in: Climate Change 2013:

469   The Physical Science Basis. Contribution of Working Group I to the Fifth Assessment Report of the Intergovernmental

470   Panel on Climate Change, edited by: Stocker, T. F., Qin, D., Plattner, G.-K., Tignor, M., Allen, S. K., Boschung, J., Nauels, A.,

471   Xia, Y., Bex, V., and Midgley, P. M., Cambridge University Press, Cambridge, United Kingdom and New York, NY, USA, 571–

472   658, 2013.

473   Brock, C. A., Wagner, N. L., Anderson, B. E., Attwood, A. R., Beyersdorf, A., Campuzano-Jost, P., Carlton, A. G., Day, D. A.,

474   Diskin, G. S., Gordon, T. D., Jimenez, J. L., Lack, D. A., Liao, J., Markovic, M. Z., Middlebrook, A. M., Ng, N. L., Perring, A. E.,

475   Richardson, M. S., Schwarz, J. P., Washenfelder, R. A., Welti, A., Xu, L., Ziemba, L. D., and Murphy, D. M.: Aerosol optical

476   properties in the southeastern United States in summer – Part 1: Hygroscopic growth, Atmos. Chem. Phys., 16, 4987-5007,

477   10.5194/acp-16-4987-2016, 2016.

478   Chen, J., Zhao, C. S., Ma, N., and Yan, P.: Aerosol hygroscopicity parameter derived from the light scattering enhancement

479   factor measurements in the North China Plain, Atmos. Chem. Phys., 14, 8105-8118, 10.5194/acp-14-8105-2014, 2014.

480   Drinovec, L., Močnik, G., Zotter, P., Prévôt, A. S. H., Ruckstuhl, C., Coz, E., Rupakheti, M., Sciare, J., Müller, T., Wiedensohler,

481   A., and Hansen, A. D. A.: The "dual-spot" Aethalometer: an improved measurement of aerosol black carbon with real-

482   time loading compensation, Atmospheric Measurement Techniques, 8, 1965-1979, 10.5194/amt-8-1965-2015, 2015.

483   Ervens, B., Cubison, M. J., Andrews, E., Feingold, G., Ogren, J. A., Jimenez, J. L., Quinn, P. K., Bates, T. S., Wang, J., Zhang,

484   Q., Coe, H., Flynn, M., and Allan, J. D.: CCN predictions using simplified assumptions of organic aerosol composition and

485   mixing state: a synthesis from six different locations, Atmos. Chem. Phys., 10, 4795-4807, 10.5194/acp-10-4795-2010,

486   2010.

487   Gunthe, S. S., King, S. M., Rose, D., Chen, Q., Roldin, P., Farmer, D. K., Jimenez, J. L., Artaxo, P., Andreae, M. O., Martin, S.

488   T., and Pöschl, U.: Cloud condensation nuclei in pristine tropical rainforest air of Amazonia: size-resolved measurements

489   and modeling of atmospheric aerosol composition and CCN activity, Atmos. Chem. Phys., 9, 7551-7575, 10.5194/acp-9-

490   7551-2009, 2009.

491   Hänel, G.: An attempt to interpret the humidity dependencies of the aerosol extinction and scattering coefficients,

492   Atmospheric Environment (1967), 15, 403-406, http://dx.doi.org/10.1016/0004-6981(81)90045-7, 1981.

493   Hennig, T., Massling, A., Brechtel, F. J., and Wiedensohler, A.: A tandem DMA for highly temperature-stabilized hygroscopic

494   particle growth measurements between 90% and 98% relative humidity, Journal of Aerosol Science, 36, 1210-1223,

495   10.1016/j.jaerosci.2005.01.005, 2005.

496   Kuang, Y., Zhao, C. S., Tao, J. C., and Ma, N.: Diurnal variations of aerosol optical properties in the North China Plain and

497   their influences on the estimates of direct aerosol radiative effect, Atmos. Chem. Phys., 15, 5761-5772, 10.5194/acp-15-

498   5761-2015, 2015.

499   Kuang, Y., Zhao, C. S., Ma, N., Liu, H. J., Bian, Y. X., Tao, J. C., and Hu, M.: Deliquescent phenomena of ambient aerosols on

500   the North China Plain, Geophys. Res. Lett., n/a-n/a, 10.1002/2016GL070273, 2016a.

501   Kuang, Y., Zhao, C. S., Tao, J. C., Bian, Y. X., and Ma, N.: Impact of aerosol hygroscopic growth on the direct aerosol radiative

502   effect in summer on North China Plain, Atmospheric Environment, 147, 224-233,

503   http://dx.doi.org/10.1016/j.atmosenv.2016.10.013, 2016b.

504   Liu, H. J., Zhao, C. S., Nekat, B., Ma, N., Wiedensohler, A., van Pinxteren, D., Spindler, G., Müller, K., and Herrmann, H.:

505   Aerosol hygroscopicity derived from size-segregated chemical composition and its parameterization in the North China

506   Plain, Atmos. Chem. Phys., 14, 2525-2539, 10.5194/acp-14-2525-2014, 2014.

507   Liu, P. F., Zhao, C. S., Göbel, T., Hallbauer, E., Nowak, A., Ran, L., Xu, W. Y., Deng, Z. Z., Ma, N., Mildenberger, K., Henning,

508   S., Stratmann, F., and Wiedensohler, A.: Hygroscopic properties of aerosol particles at high relative humidity and their

509   diurnal variations in the North China Plain, Atmos. Chem. Phys., 11, 3479-3494, 10.5194/acp-11-3479-2011, 2011.

510   Müller, T., Laborde, M., Kassell, G., and Wiedensohler, A.: Design and performance of a three-wavelength LED-based total

511   scatter and backscatter integrating nephelometer, Atmos. Meas. Tech., 4, 1291-1303, 10.5194/amt-4-1291-2011, 2011.

512   Ma, N., Zhao, C. S., Müller, T., Cheng, Y. F., Liu, P. F., Deng, Z. Z., Xu, W. Y., Ran, L., Nekat, B., van Pinxteren, D., Gnauk, T.,

513   Müller, K., Herrmann, H., Yan, P., Zhou, X. J., and Wiedensohler, A.: A new method to determine the mixing state of light

514   absorbing carbonaceous using the measured aerosol optical properties and number size distributions, Atmos. Chem. Phys.,

515   12, 2381-2397, 10.5194/acp-12-2381-2012, 2012.

516   Petters, M. D., and Kreidenweis, S. M.: A single parameter representation of hygroscopic growth and cloud condensation

517   nucleus activity, Atmospheric Chemistry and Physics, 7, 1961-1971, 2007.

518   Pinnick, R. G., Jennings, S. G., and Chýlek, P.: Relationships between extinction, absorption, backscattering, and mass

519   content of sulfuric acid aerosols, Journal of Geophysical Research: Oceans, 85, 4059-4066, 10.1029/JC085iC07p04059,

520   1980.

521   Seinfeld, J. H., and Pandis, S. N.: Atmospheric chemistry and physics: from air pollution to climate change, John Wiley &

522   Sons, 2006.

523   Tao, J. C., Zhao, C. S., Ma, N., and Liu, P. F.: The impact of aerosol hygroscopic growth on the single-scattering albedo and

524   its application on the NO2 photolysis rate coefficient, Atmos. Chem. Phys., 14, 12055-12067, 10.5194/acp-14-12055-2014,

525   2014.

526   Titos, G., Cazorla, A., Zieger, P., Andrews, E., Lyamani, H., Granados-Muñoz, M. J., Olmo, F. J., and Alados-Arboledas, L.:

527   Effect of hygroscopic growth on the aerosol light-scattering coefficient: A review of measurements, techniques and error

528   sources, Atmospheric Environment, 141, 494-507, http://dx.doi.org/10.1016/j.atmosenv.2016.07.021, 2016.

529   Wex, H., Neususs, C., Wendisch, M., Stratmann, F., Koziar, C., Keil, A., Wiedensohler, A., and Ebert, M.: Particle scattering,

530   backscattering, and absorption coefficients: An in situ closure and sensitivity study, Journal of Geophysical Research-

531   Atmospheres, 107, 18, 10.1029/2000jd000234, 2002.

532   Wu, Z. J., Zheng, J., Shang, D. J., Du, Z. F., Wu, Y. S., Zeng, L. M., Wiedensohler, A., and Hu, M.: Particle hygroscopicity and

533   its link to chemical composition in the urban atmosphere of Beijing, China, during summertime, Atmos. Chem. Phys., 16,

534   1123-1138, 10.5194/acp-16-1123-2016, 2016.

535   You, Y., Smith, M. L., Song, M., Martin, S. T., and Bertram, A. K.: Liquid–liquid phase separation in atmospherically relevant

536   particles consisting of organic species and inorganic salts, International Reviews in Physical Chemistry, 33, 43-77,

537   10.1080/0144235X.2014.890786, 2014.

538   Zhao, C., Tie, X., and Lin, Y.: A possible positive feedback of reduction of precipitation and increase in aerosols over eastern

539   central China, Geophys. Res. Lett., 33, L11814, 10.1029/2006GL025959, 2006.

540   Zieger, P., Fierz-Schmidhauser, R., Weingartner, E., and Baltensperger, U.: Effects of relative humidity on aerosol light

541   scattering: results from different European sites, Atmos. Chem. Phys., 13, 10609-10631, 10.5194/acp-13-10609-2013,

542   2013.

543

544

545

546

547

548

549

550

551

552

553

554

555

556

557

558

559

560

561

562

563 **Table 1**. Locations, time periods and used datasets of five field campaigns

Location	Wuqing	Wuqing	Xianghe	Wangdu	Gucheng
Time period	7 march to 4 April, 2009	12 July to 14 August, 2009	9 July to 8 August, 2013	4 June to 14 July, 2014	15 October to 25 November, 2016
PNSD	TSMPS+APS	TSMPS+APS	TSMPS+APS	TSMPS+APS	SMPS+APS
BC	MAAP	MAAP	MAAP	MAAP	AE33
σ_{sp}	TSI 3563	TSI 3563	TSI 3563	TSI 3563	Aurora 3000
f(RH)				Humidified nephelometer system	Humidified nephelometer system
g(RH)				HH-TDMA	

564

565

566

567

568

569

570

571

572

573

574

575

576

577
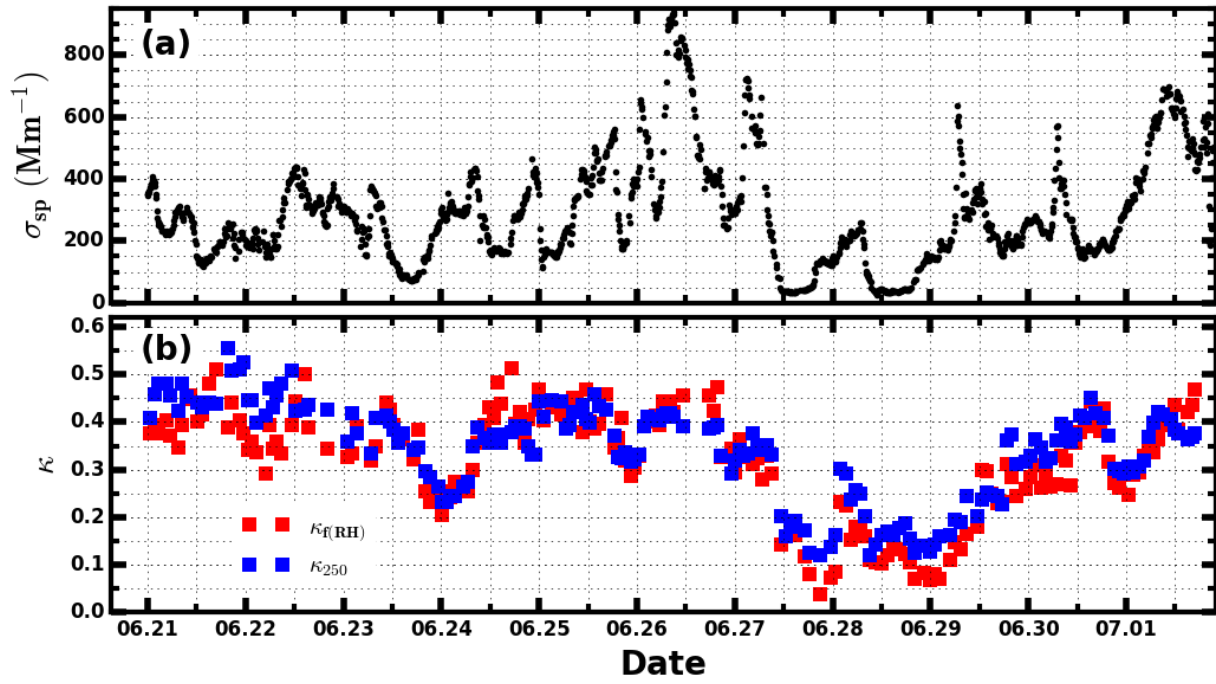
Figure 1. (a) The time series of σ_{sp} at 550 nm;   (b) The time series of κ values derived from $f(\text{RH})$ measurements ($\kappa_{f(\text{RH})}$) by combining information of PNSD and BC, and time series of average κ values of aerosol particles at 250 nm (κ_{250}) which is calculated from measurements of HH-TDMA.

581

582

583

584
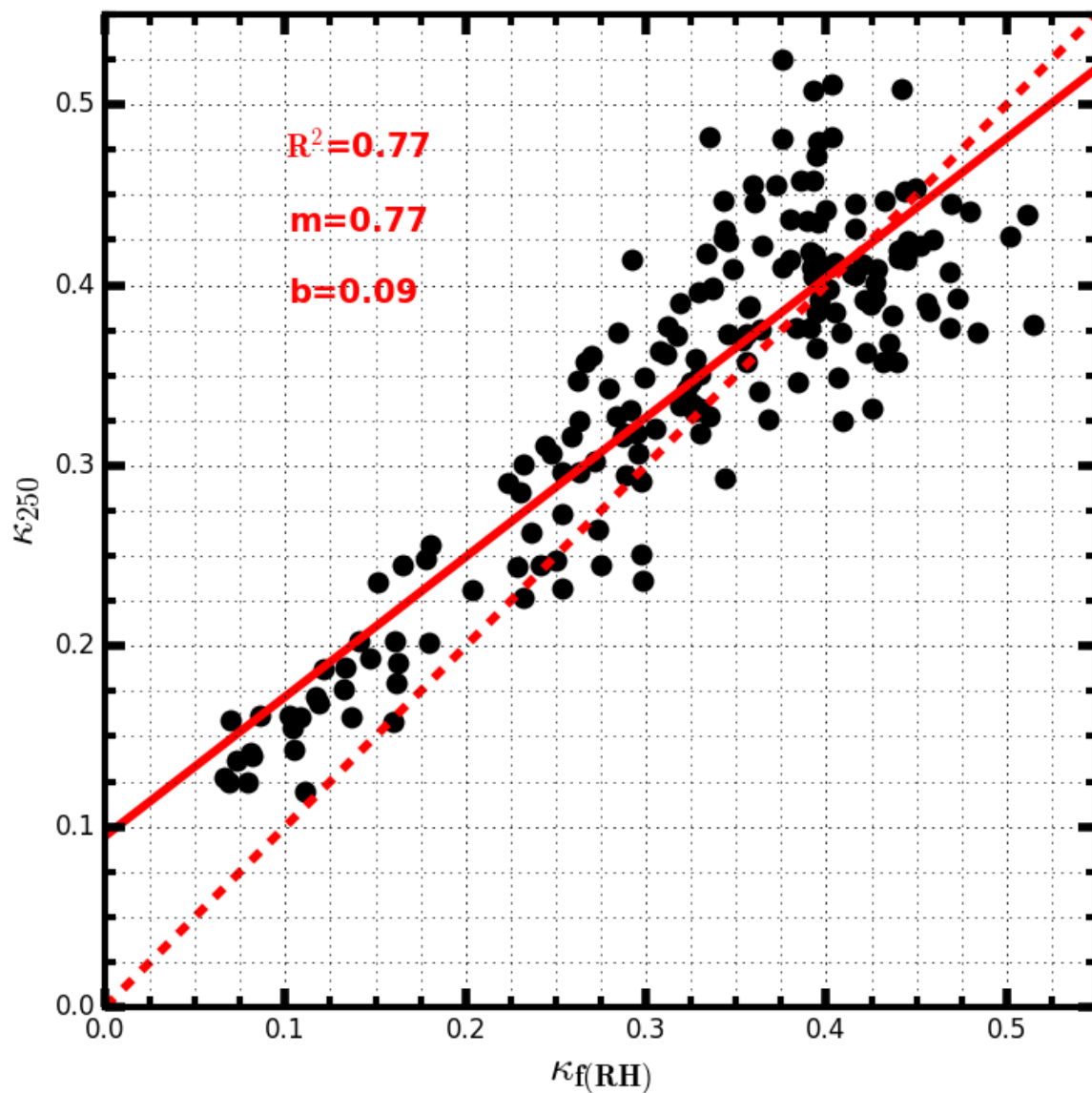
585 **Figure 2**. The comparison between κ values derived from $f(\mathrm{RH})$ measurements ($\kappa_{f(\mathrm{RH})}$) and average κ values

586 for aerosol particles with a diameter of 250 nm (κ_{250}) which are derived from measurements of HH-TDMA. R^2 is

587 the square of correlation coefficient, m is the slope and b is the intercept.

588

589

590

591
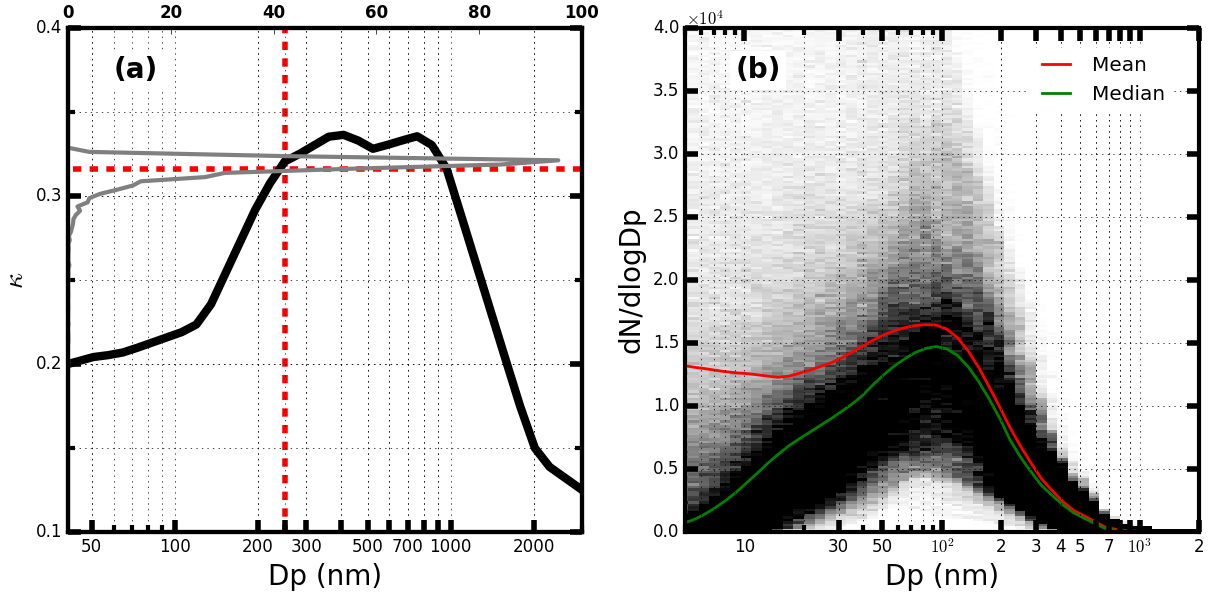
Figure 3. (a) The thick black line represents the average size-resolved κ distribution from HaChi campaign. The solid gray line represents the probability distribution of retrieved κ values with this size-resolve κ distribution by using all PNSDs shown in figure (b), and the horizontal dashed line represents their average. The vertical dashed red line represents the position of 250 nm. (b) All PNSDs which are observed from three different representative background sites of the NCP during summer, they are used to model relationship between size-resolved κ and retrieved κ values from $f(\text{RH})$ measurements, and the gray color represents the frequency of PNSD, darker point corresponds to higher frequency, red and green line represent mean of median values of all observed PNSDs.

599

600
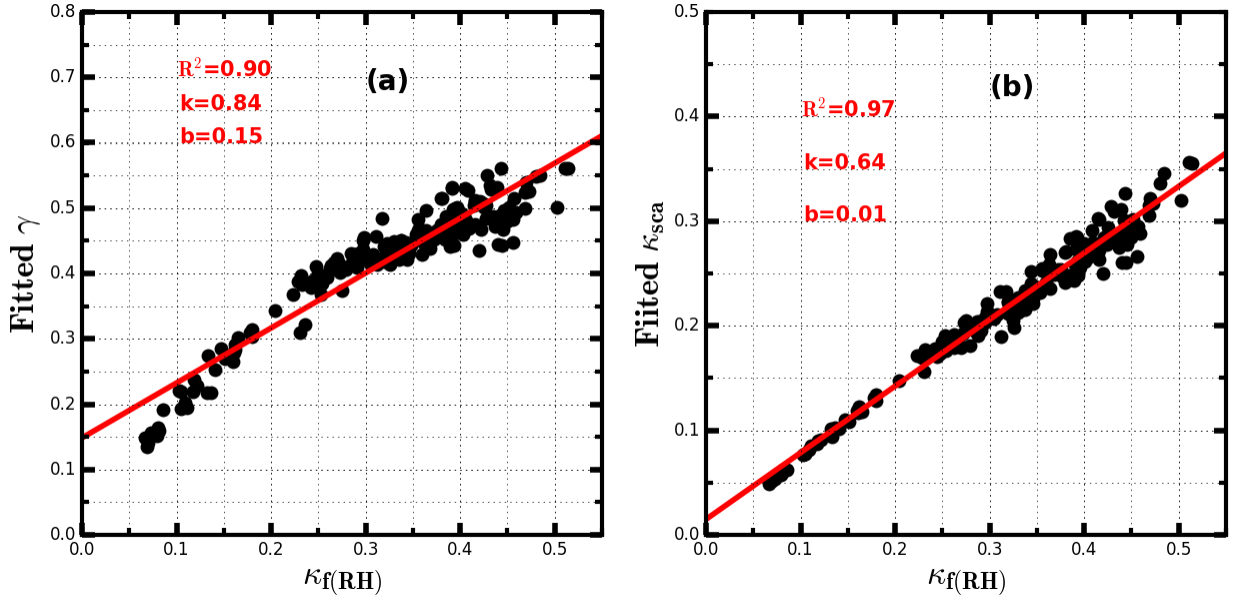
Figure 4. (a) The linear relationship between values of $\kappa_{f(\text{RH})}$ and fitted γ, R^2 is the square of correlation coefficient, k is the slope and b is the intercept; (b) The linear relationship between values of $\kappa_{f(\text{RH})}$ and fitted κ_{sca}.

603

604

605

606
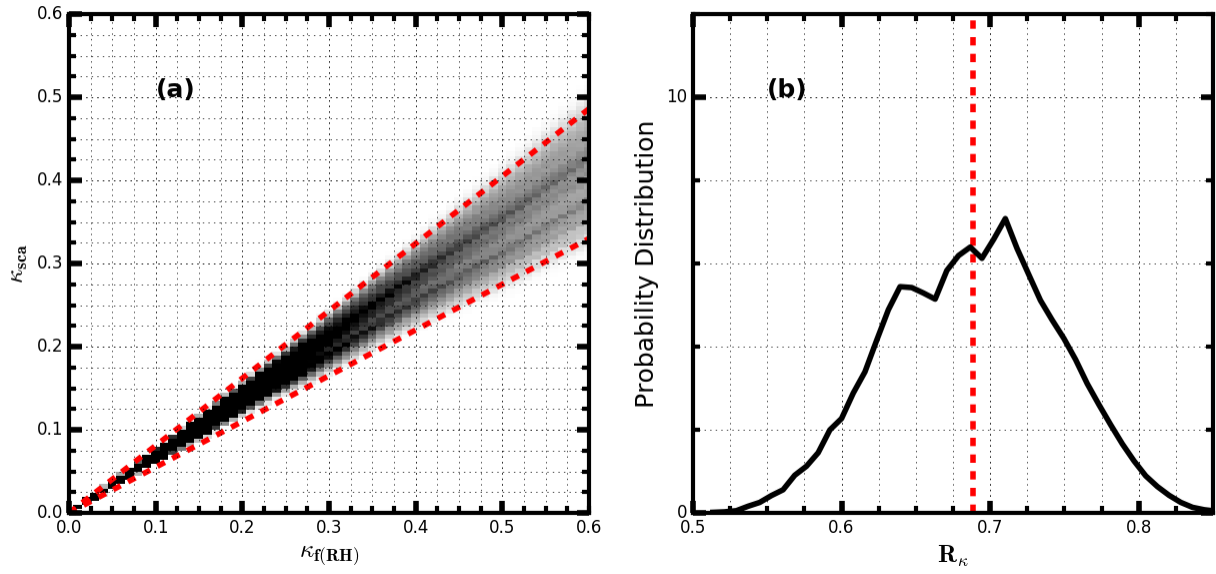
Figure 5. (a) Simulated relationships between $\kappa_{f(\mathrm{RH})}$ and κ_{sca} under different PNSD conditions (all PNSDs shown in Fig.3a are used as inputs to conduct the simulation experiment), gray color represents the frequency and darker point corresponds to higher frequency, the slope of two dashed lines are 0.55 and 0.81; (b) The probability distribution of R_κ ($\kappa_{sca}/\kappa_{f(\mathrm{RH})}$).

626
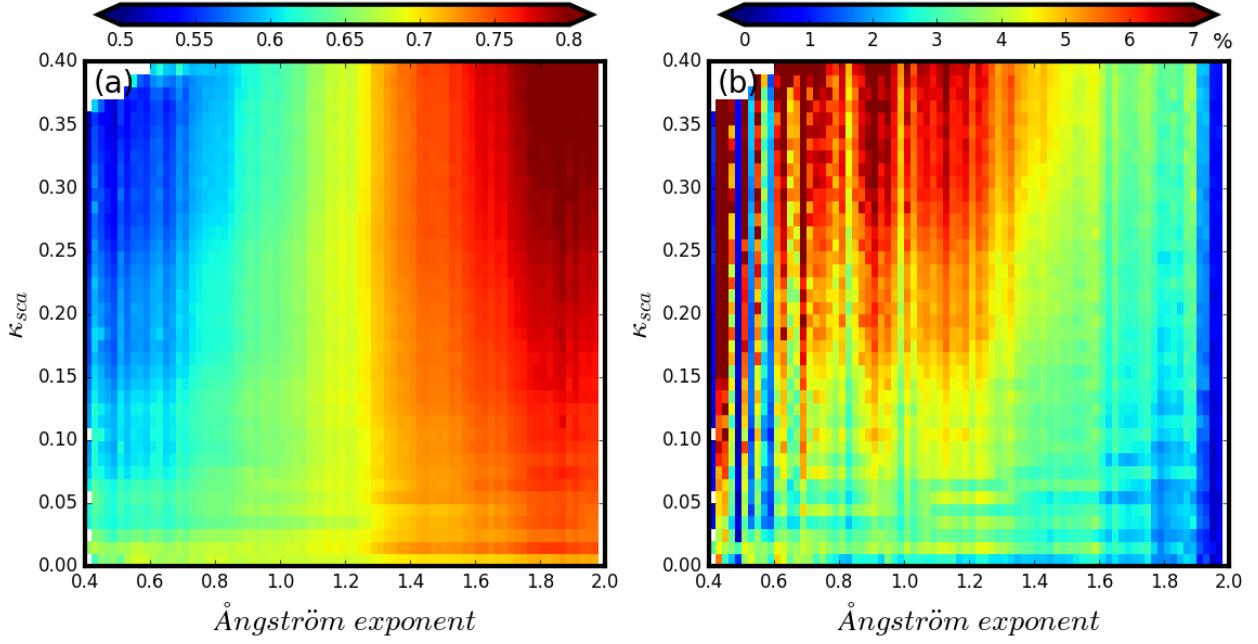
Figure 6. (a) Colors represent R_κ values and the color bar is shown on the top of this figure, x-axis represents Ångström exponent and y-axis represents κ_{sca}. (b) Meanings of x-axis and y-axis are same with them in (a), however, color represents the percentile value of the standard deviation of R_κ values within each grid divided by their average.

631

632

633
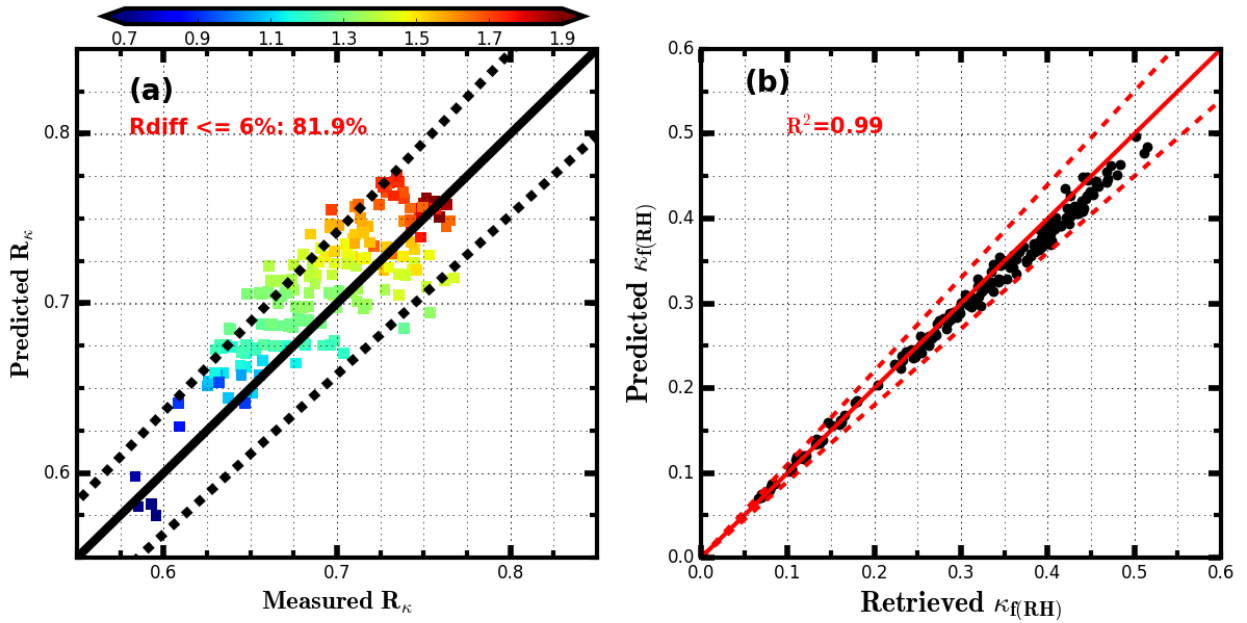
Figure 7. (a) The comparison between measured and predicted R_κ values, colors represent values of Ångström exponent, texts with red color show the percentile of points with relative difference (Rdiff) less than 6% , two dashed line are 6% relative difference lines ; (b) the comparison between $\kappa_{f(RH)}$ retrieved from Method 1 and predicted $\kappa_{f(RH)}$ by using the new method introduced in Sect.4.3, R^2 is the square of correlation coefficient, two dashed lines are 10% relative difference lines.

639
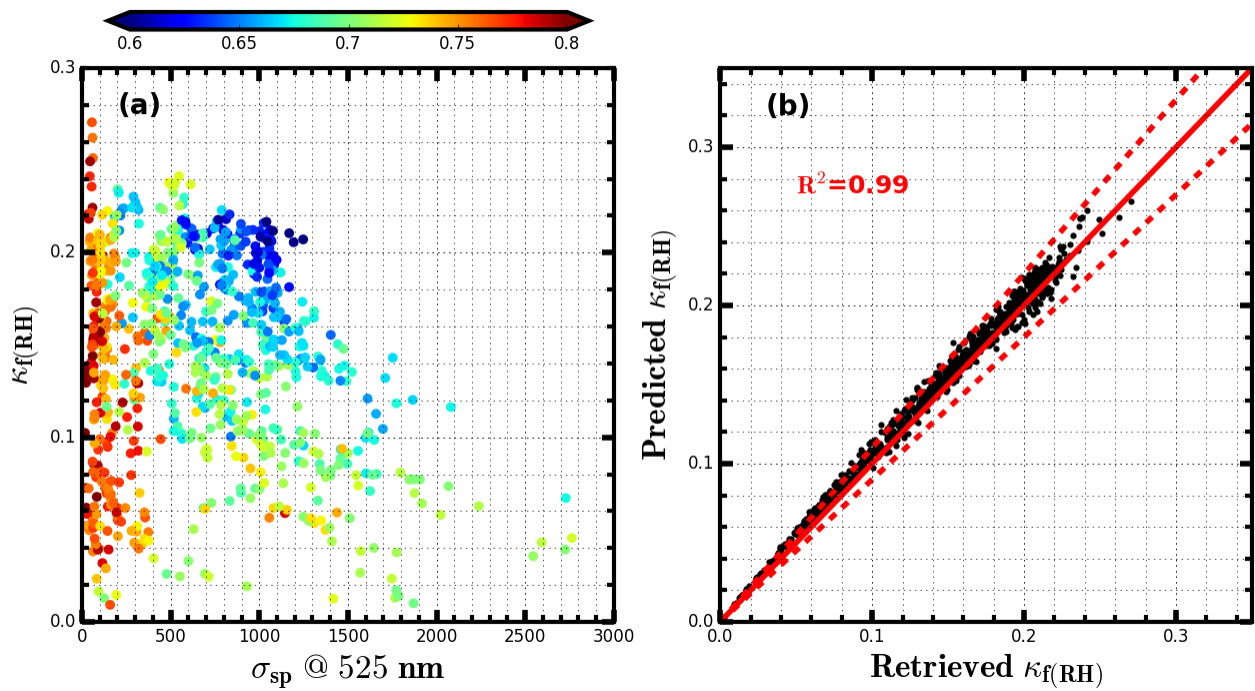
640

641 **Figure 8**. (a) x axis represents σ_{sp} at 525 nm (Mm^{-1}), y axis represents retrieved $\kappa_{f(RH)}$, colors of scatter points
642 represent corresponding values of R_κ; (b) The comparison between $\kappa_{f(RH)}$ retrieved from Method 1 and predicted
643 $\kappa_{f(RH)}$ by using the new method, R^2 is the square of correlation coefficient, two dashed red lines represent 10%
644 deviations from 1:1 line.